Temperature Dependence for the Rate Coefficients of the Reactions of the OH Radical with a Series of Formates

Stéphane Le Calvé, Georges Le Bras, and Abdelwahid Mellouki*

Laboratoire de Combustion et Systèmes Réactifs, CNRS and Université d'Orléans, 45071 Orléans Cedex 2, France

Received: February 13, 1997[⊗]

The kinetics of the reactions of OH with methyl formate (1), ethyl formate (2), *n*-propyl formate (3), *n*-butyl formate (4), and *tert*-butyl formate (5) were studied using the pulsed laser photolysis−laser-induced fluorescence technique. The obtained results in the temperature range 233−372 K were the following (in cm^3 $molecule^{-1}$ s^{-1}): $k_1 = (8.54 \pm 1.98) \times 10^{-13} \exp[-(461 \pm 70)/T]$, $k_2 = (5.66 \pm 1.10) \times 10^{-13} \exp[(134 \pm 53)/T]$, $k_3 = (1.65 \pm 0.45) \times 10^{-12} \exp[(42 \pm 78)/T]$, $k_4 = (3.63 \pm 1.08) \times 10^{-12} \exp[(15 \pm 88)/T]$, and $k_5 = (3.59 \pm 0.98) \times 10^{-12} \exp[-(449 \pm 82)/T]$. At room temperature the obtained rate coefficients were the following (in 10^{-13} cm^3 $molecule^{-1}$ s^{-1}): $k_1 = 1.73 \pm 0.21$; $k_2 = 8.52 \pm 0.75$; $k_3 = 18.0 \pm 1.7$; $k_4 = 35.4 \pm 5.2$; and $k_5 = 7.46 \pm 0.91$. These results are discussed with respect to literature data and structure−activity relationships.

Introduction

Oxygenated compounds are widely used in paints, as solvents and degreasing agents. Esters are an important class of these oxygenated compounds. Esters are used as food flavorings and in perfumes, and they are also present in some fruits and can be then emitted to the atmosphere naturally. They are also produced in the tropospheric degradation of some volatile organic compounds. For example, methyl formate and ethyl formate are the most important products of the tropospheric degradation of dimethyl ether and diethyl ether, respectively.[1,2] The atmospheric degradation of the two fuel additives, methyl *tert*-butyl ether (MTBE) and ethyl *tert*-butyl ether (ETBE), yields mainly *tert*-butyl formate.[1−5]

The role of these formates in the formation of tropospheric ozone and other secondary pollutants is of some concern. The tropospheric photochemical reactivity of formates is controlled mainly by their reaction with OH radicals. Their reaction with NO_3 radicals,[6] or O_3,[7] and the tropospheric photolysis[8] are slow processes and are thus negligible in the atmospheric degradation of the formates. In order to assess the potential impact of this class of VOCs on air quality, rate coefficients data for their reaction with OH are needed.

We report in this paper the absolute rate coefficients for the reactions of the OH radical with five formates, methyl formate, ethyl formate, *n*-propyl formate, *n*-butyl formate, and *tert*-butyl formate, in the temperature range 233−372 K:

$$OH + HC(O)OCH_3 \rightarrow \text{products} \quad (1)$$

$$OH + HC(O)OC_2H_5 \rightarrow \text{products} \quad (2)$$

$$OH + HC(O)OC_3H_7 \rightarrow \text{products} \quad (3)$$

$$OH + HC(O)OC_4H_9 \rightarrow \text{products} \quad (4)$$

$$OH + HC(O)OC(CH_3)_3 \rightarrow \text{products} \quad (5)$$

A few studies have been carried out so far on the reactions of OH with formates. The present work provides the first measurements of the temperature dependence of the rate constants for the reaction of OH with these formates.

Experimental Section

The apparatus and experimental techniques used have been described in detail previously[9,10] and are briefly discussed here. The pulsed laser photolysis−laser-induced fluorescence (PLP-LIF) technique was used. Two sources were used to generate OH radicals: photolysis of H_2O_2 at $\lambda = 248$ nm (KrF excimer laser) and photolysis of HONO at $\lambda = 351$ nm (XeF excimer laser). The concentration of hydroxyl radicals was monitored at various reaction times ranging from ca. 10 μs to 10 ms by pulsed laser induced fluorescence. A Nd:YAG pumped frequency-doubled dye laser was used to excite the OH radical at $\lambda = 282$ nm. Fluorescence from the OH radical was detected by a photomutiplier, fitted with a 309 nm narrow bandpass filter. The output pulse from the photomultiplier was integrated for a preset period by a gated charge integrator. Typically the fluorescence signal from 10 to 15 different delay times from 100 probe laser shots were averaged to generate OH concentration−time profiles over at least three lifetimes. Formate/H_2O_2 or formate/HONO mixtures in helium diluent were flowed slowly through the cell, so that each photolysis/probe sequence interrogates a fresh gas mixture and reaction products did not build up in the cell.

All experiments were carried out under pseudo-first-order conditions with [formate] ≫ $[OH]_0$, the initial concentration of OH being $[OH]_0 < 2 \times 10^{11}$ molecule cm^{-3}. The temporal profiles of [OH], therefore, followed the pseudo-first-order rate law:

$$[OH]_t = [OH]_0 e^{-k't}$$

where $k' = k_i[X_i] + k'_0$. X_i refers to the formate in reaction i ($i = 1-5$) and k_i is the rate coefficient for the reaction of OH with the formate (i). The decay rate, k'_0, is the first-order OH decay rate constant in the absence of the formate. The value of k'_0 is essentially the sum of the reaction rate of OH with its precursor (H_2O_2 or HONO) and the diffusion rate of OH out of the detection zone. The concentrations of OH at various reaction times (delay between the photolysis pulses and the probe pulses) were determined by measuring the LIF signal intensities at those

[⊗] Abstract published in *Advance ACS Abstracts,* July 1, 1997.

S1089-5639(97)00554-9 CCC: $14.00

delay times. Weighted (according to the signal to noise of the measured signal at the given time) least-squares analysis were used to fit the data to the above equation and extract the values of k'. The second-order rate coefficients (k_i) were obtained from the measured values of k' at various concentrations of formates.

The helium carrier gas (UHP certified to >99.9995% (Alphagas)) was used without purification. The 50 wt % H_2O_2 solution, obtained from Prolabo, was concentrated by bubbling helium through the solution to remove water for several days prior to use and constantly during the course of the experiments. It was admitted into the reaction cell by passing a small flow of helium through a glass bubbler containing H_2O_2. HONO was produced in situ by reacting $NaNO_2$ (0.1 M) with diluted H_2SO_4 (10%) contained in a stirred round bottomed flask. The effluent from the flask was swept into the cell by a known flow of helium. Methyl formate (>99%) and ethyl formate (>98%) were from Fluka, *n*-propyl formate (≈98.7%), *n*-butyl formate (>97%), and *tert*-butyl formate (>99%) were from Aldrich. These compounds were further purified by repeated freeze, pump, and thaw cycles and fractional distillation before use.

For the kinetic measurements, the studied formates were premixed with helium in a 10 L glass light-tight bulb to form 1−23% mixture at a total pressure of ≈800 Torr. All the gases flowed into the reactor through Teflon tubing. The gas mixture containing the formate, the photolytic precursor (H_2O_2 or HONO), and the bath gas (approximately 100 Torr of helium) were flowed through the cell with a linear velocity ranging between 5 and 20 cm s^{-1}. The concentrations of the formates were calculated from their mass flow rates, the temperature, and the pressure in the reaction cell. All flow rates were measured with mass flowmeters calibrated by measuring the rate of pressure increase in a known volume. The pressure in the cell was measured with a capacitance manometer connected at the cell entrance.

Results and Discussion

For the studied formates, except methyl formate, the OH decay plots, ln[OH] = $f(t)$, showed excellent linearity when H_2O_2 was used as the OH precursor. The experiments were, therefore, performed with this OH source for ethyl formate, *n*-propyl formate, *n*-butyl formate, and *tert*-butyl formate. In contrast, some complications were apparent with methyl formate using H_2O_2 as the source of OH. The OH decay plots in the presence of methyl formate were curved. However, the OH concentration was sufficiently low ($[OH]_0 < 2 \times 10^{11}$ molecule cm^{-3}) and the purity of methyl formate was at a level (>99%) that secondary reactions of OH with a product of the reaction or from the impurities were negligible and could not explain the observed curvature of the plots. The possible role of photodissociation products of methyl formate was also considered. The reported UV spectrum of methyl formate[8] shows that this compound does absorb slightly at $\lambda = 248$ nm. We have remeasured the UV absorption cross section using a diode array spectrometer.[11] The obtained value at 248 nm is $\sigma_{HC(O)OCH_3} = (7.74 \pm 0.75) \times 10^{-21}$ cm^2 $molecule^{-1}$. This value is in excellent agreement with that previously reported at $\lambda = 248$ nm: $\sigma_{HC(O)OCH_3} = 7.9 \times 10^{-21}$ cm^2 $molecule^{-1}$.[8] Using this value, we can calculate that under our experimental conditions up to 10^{11} molecule cm^{-3} of photoproducts could be produced in the photolysis cell. Photofragment production was confirmed by observing a fluorescence signal in the absence of H_2O_2. Typical temporal profiles are shown in Figure 1 where the fluorescence signal intensity was plotted as function of the delay time between the two laser shots (photolysis and LIF shots) for different concentrations of methyl formate. It is suggested that this signal is probably due to the fluorescence of CH_3O which has been previously identified as a photolysis product of $HC(O)OCH_3$ around 248 nm.[8,12] Then, in order to avoid complications in our kinetic studies, we used radiation of wavelength 351 nm to generate OH from the photolysis of HONO. Methyl formate does not absorb at this wavelength.[8] Under these conditions, the OH decay plots, ln[OH] = $f(t)$, showed excellent linearity.

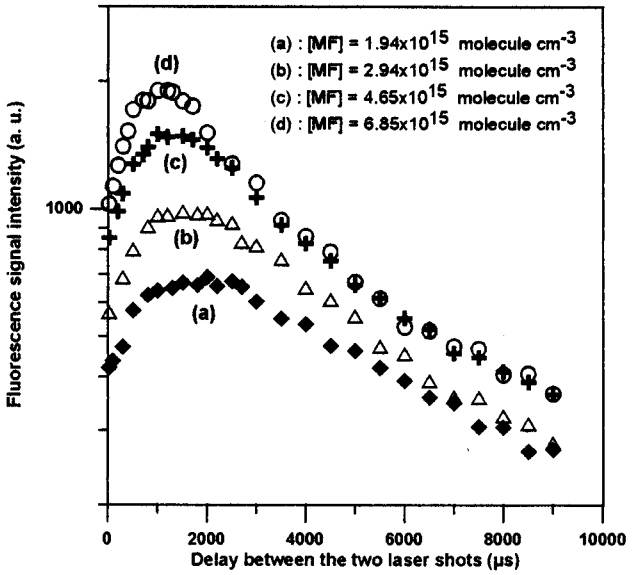

Figure 1. Observed fluorescence signal obtained from the photolysis of different concentrations of $HC(O)OCH_3$ ([MF]) in helium at λ = 248 nm versus the delay between the photolysis and excitation at λ = 282 nm. This signal is assigned to the fluorescence of CH_3O around 310 nm (see text).

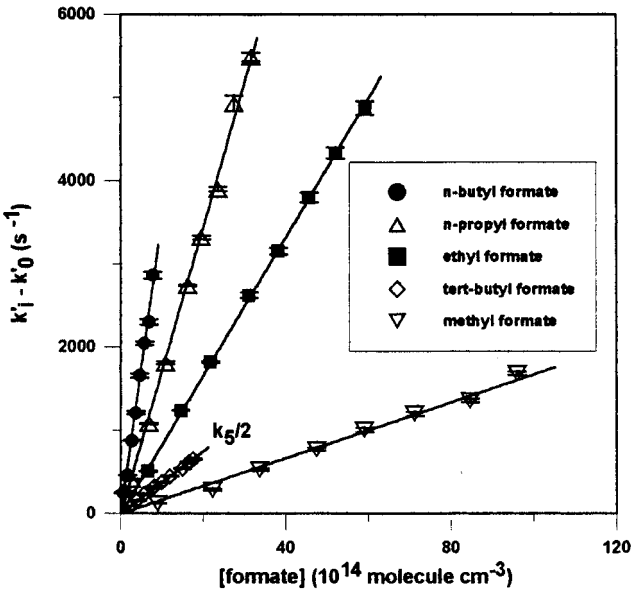

Figure 2. Plots of $k'_i - k'_o$ vs formate concentration at room temperature (i = 1−5). The lines represent the linear least-squares fitting.

Possible contributions to the measured rate constants from secondary reactions of OH with the products of reactions 1−5 were significantly reduced by using high (10^2−10^4) [formate]/[OH] ratios. As expected, the values of k_1 were independent of the OH radical concentration. The rate constants were also shown to be independent of variations in the flow velocity through the reactor, changes in the total pressure of the system, or variations in the photolysis laser fluence (at 248 or 351 nm). Values of k_i were derived from the least-squares fit of the straight

TABLE 1: Reactions OH + Methyl Formate (1), OH + Ethyl Formate (2), OH + *n*-Propyl Formate (3), OH + *n*-Butyl Formate (4), and OH + *tert*-Butyl Formate (5): Summary of Experimental Conditions and Measured k_1, k_2, k_3, k_4, and k_5

T (K)	[methyl formate] (10^{14})[a]	$10^{13} \times (k_1 \pm 2\sigma)$[b]	[ethyl formate] (10^{14})[a]	$10^{13} \times (k_2 \pm 2\sigma)$[b]	[*n*-propyl formate] (10^{14})[a]	$10^{12} \times (k_3 \pm 2\sigma)$[b]	[*n*-butyl formate] (10^{14})[a]	$10^{12} \times (k_4 \pm 2\sigma)$[b]	[*tert*-butyl formate] (10^{14})[a]	$10^{13} \times (k_5 \pm 2\sigma)$[b]
233	8.12−79.76	1.29 ± 0.06								
243			4.65−31.35	10.26 ± 0.39						
253	7.83−84.51	1.39 ± 0.06	7.06−72.45	9.70 ± 0.11	3.40−36.49	1.95 ± 0.06	0.53−7.95	4.30 ± 0.26	2.68−21.39	6.20 ± 0.24
253	11.57−72.76	1.38 ± 0.11	8.03−55.96	9.80 ± 0.25[d]	6.45−58.05	2.08 ± 0.05[d]	0.16−2.34	3.91 ± 0.32	7.09−49.93	6.34 ± 0.75[e]
263			6.48−69.24	9.12 ± 0.33	2.77−28.58	1.99 ± 0.03	0.61−8.64	3.82 ± 0.34	2.56−21.53	6.87 ± 0.25
263							0.60−8.48	4.06 ± 0.22		
263							0.52−7.39	4.06 ± 0.39		
273	6.79−76.51	1.56 ± 0.05	6.29−67.22	8.90 ± 0.42	3.33−33.91	1.87 ± 0.04	0.51−8.03	4.06 ± 0.14	2.24−17.67	6.98 ± 0.32
273							0.47−8.72	3.55 ± 0.32		
283							0.46−8.07	3.47 ± 0.28		
297							0.42−7.80	3.56 ± 0.34[c]		
298	5.79−54.84	1.80 ± 0.07	6.48−59.04	8.43 ± 0.32	2.53−31.48	1.73 ± 0.08	0.49−7.65	3.61 ± 0.23	1.66−19.98	7.29 ± 0.43
298	7.41−86.58	1.60 ± 0.12	6.14−64.22	8.32 ± 0.27	2.82−25.77	1.82 ± 0.04	0.42−8.32	3.45 ± 0.18	2.39−17.41	7.46 ± 0.30
298	10.89−105.53	1.82 ± 0.09	3.55−37.25	8.82 ± 0.32[c]	2.67−25.24	1.86 ± 0.05[c]			2.19−20.53	7.50 ± 0.52
298	8.76−95.91	1.69 ± 0.12[f]							3.60−32.16	7.58 ± 0.54[d]
298	21.05−102.04	1.75 ± 0.07[d]								
313							0.47−7.67	3.64 ± 0.32		
323	8.77−96.58	1.95 ± 0.13	5.79−59.03	8.30 ± 0.32	2.79−29.14	1.74 ± 0.09			2.12−16.07	8.87 ± 0.52
333							0.42−6.17	3.82 ± 0.22		
333							0.36−7.00	3.75 ± 0.18		
348	8.38−90.08	2.25 ± 0.09	5.87−55.00	8.51 ± 0.53	2.69−27.28	1.87 ± 0.06			2.17−16.47	10.25 ± 0.82
348	9.05−69.14	2.41 ± 0.10								
353							0.40−5.84	3.95 ± 0.28		
371							0.35−5.71	4.10 ± 0.16		
372	7.89−82.83	2.48 ± 0.08	4.98−51.36	8.74 ± 0.36	2.43−25.32	1.92 ± 0.04			2.19−15.04	11.15 ± 0.83
372	18.61−105.22	2.71 ± 0.12[e]	9.24−63.88	8.41 ± 0.58[e]	4.59−44.53	2.00 ± 0.11[e]			1.89−14.11	11.63 ± 0.64[c]

[a] Units of molecule cm^{-3}. [b] Units of cm^3 molecule^{-1} s^{-1}. [c] Variation of the photolysis laser fluence (decrease by a factor of 3). [d] Variation of flow velocity (decrease by a factor of 3). [e] Experiments carried out at 300 Torr. [f] Variation of the photolysis laser fluence (decrease by a factor of 2).

lines. Figure 2 shows the plots of k_i versus the formate concentration obtained at room temperature for the different formates. The quoted errors for k_i determined in this work include 2σ from the least-squares analysis and the estimated systematic error 5% (due to uncertainties in measured concentrations).

The experimental conditions and the measured values of the rate coefficients over the temperature range 233−372 K are listed in Table 1. They are also shown in Figure 3 in the conventional form of the Arrhenius equation ($k = Ae^{-E_a/RT}$). The Arrhenius parameters for the OH reactions with the formates are given in Table 2 together with those from previous studies. For each reaction, only one previous study has been carried out at room temperature.[4,13] Agreement between the rate constant for reaction of OH with *tert*-butyl formate obtained in this study and that derived from relative rate measurements by Smith et al.[4] is excellent. The rate constants for methyl, ethyl, and *n*-propyl formates are consistently lower (~25%) than those reported by Wallington et al.,[13] although the value for *n*-butyl formate is slightly higher than found by these workers.

Trends in the OH + Formate Reaction Rate Constants. For *n*-alkyl formates, the observed increase of the rate constants (k_1−k_4) at 298 K with the number of carbon atoms in the alkyl group indicates that the OH radical reacts predominantly with the alkoxy group.

The present values of k_1−k_5 can be compared with the rate constants previously obtained in our laboratory for the corresponding acetates[14,15] (in parentheses): $k_1 = 1.73$ (3.20), $k_2 = 8.52$ (16.7), $k_3 = 18.0$ (34.2), $k_4 = 35.4$ (55.2), $k_5 = 7.46$ (5.60), (in units of 10^{-13} cm^3 molecule^{-1} s^{-1} at 298 K). The *n*-alkyl formates are 36−49% less reactive than the corresponding formates, while *tert*-butyl formate is ca. 30% more reactive than *tert*-butyl acetate. The rate constants for these acetates agree well with the ones calculated from the structure−activity relationship (SAR) of Atkinson based on group reactivity.[16] In the updated SAR data base[16] the substituent factor for the

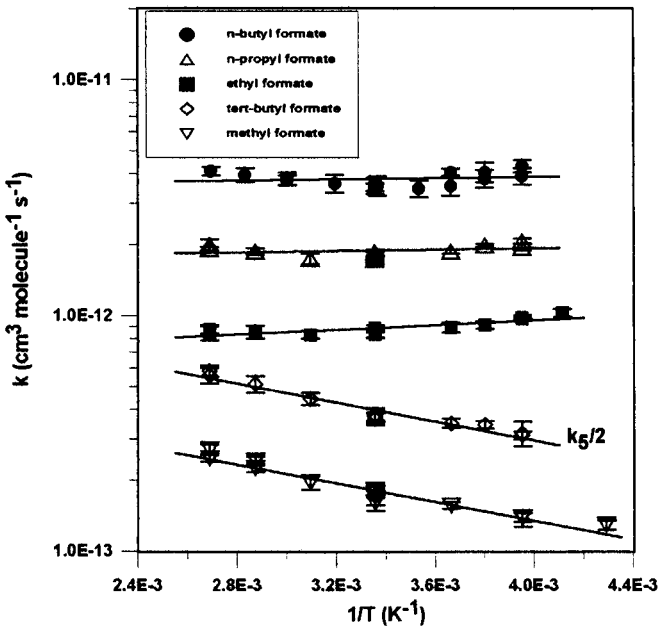

Figure 3. Plots of k_1 to k_5 vs $1/T$. The solid lines represent the two-parameter least-squares fits to the individual data points for each formate. The error bars of the individual point are 2σ and do not include estimated systematic errors.

−OC(O)R group was calculated to be F(−OC(O)R) = 1.6 at 298 K, R being an alkyl radical.

Similar SAR calculations for k_1−k_5 (OH + formate reactions), assuming that H-atom abstraction from the −OC(O)H group is negligible, give values which differ significantly from the experimental ones. The calculated values are in parentheses: $k_1 = 1.73$ (2.18), $k_2 = 8.52$ (16.6), $k_3 = 18.0$ (31.5), $k_4 = 35.4$ (45.7), $k_5 = 7.46$ (5.03). The lower experimental values for k_1−k_4 compared to calculated ones suggest that the substituent factor for the −OC(O)H group, F(−OC(O)H) is lower than

TABLE 2: Comparison of OH Reaction Rate Coefficients with Previous Work

molecule	*T*, K	k^a, 10^{12} cm^3 molecule^{-1} s^{-1}	A,^{a,b} 10^{-12} cm^3 molecule^{-1} s^{-1}	E/R,^{a,b} K	*T* range, K	technique^c	reference
$HC(O)OCH_3$	296	0.227 ± 0.034				FP-RF	13
	298	0.173 ± 0.021	0.854 ± 0.198	461 ± 70	233−372	LP-LIF	this work
$HC(O)OC_2H_5$	296	1.02 ± 0.14				FP-RF	13
	298	0.852 ± 0.075	0.566 ± 0.110	-134 ± 53	243−372	LP-LIF	this work
$HC(O)OC_3H_7$	296	2.38 ± 0.27				FP-RF	13
	298	1.80 ± 0.17	1.65 ± 0.45	-42 ± 78	253−372	LP-LIF	this work
$HC(O)OC_4H_9$	296	3.12 ± 0.33				FP-RF	13
	298	3.54 ± 0.52	3.63 ± 1.08	-15 ± 88	253−371	LP-LIF	this work
$HC(O)OC(CH_3)_3$	297	0.737 ± 0.005				RR	4
	298	0.746 ± 0.091	3.59 ± 0.98	449 ± 82	253−372	LP-LIF	this work

[a] Errors are those given by the authors. [b] For our data, the uncertainties for A and E/R were given by $\Delta A = 2A\sigma_{\ln A}$ and $\Delta E/R = 2\ \sigma_{E/R}$ for the Arrhenius forms. [c] Key: LP-LIF, laser photolysis−laser-induced fluorescence; FP-RF, flash photolysis−resonance fluorescence; RR, relative rate.

F(−OC(O)R) = 1.6. Further, hydrogen abstraction from the formate group may make a significant contribution to the overall rate constants k_1 and k_5 for the reactions of OH with methyl formate and *tert*-butyl formate which only contain low reactive CH_3 groups. Taking a mean value of F(−OC(O)H) = 0.6, derived from the fitting of experimental and SAR calculated values of k_2, k_3 and k_4, a value of 0.9×10^{-13} cm^3 molecule^{-1} s^{-1} is obtained for the partial rate constant corresponding to H-atom abstraction from the −OC(O)H group in methyl formate. This process will then contribute to ca. 50% of the overall reaction in methyl formate. For the *n*-alkyl formates, the experimental rate constants obtained at 298 K compare relatively well with the calculated ones in brackets using F(−OC(O)H) = 0.6 and k(−OC(O)H) = 0.9×10^{-13} cm^3 molecule^{-1} s^{-1}: k_1 = 1.73 (1.72), k_2 = 8.52 (8.18), k_3 = 18.0 (21.0), k_4 = 35.4 (34.2) (in units of 10^{-13} cm^3 molecule^{-1} s^{-1}).

Similarly, for *tert*-butyl formate, the difference between experimental and SAR calculated k_5 (7.46 − 5.03 = 2.43, in units of 10^{-13} cm^3 molecule^{-1} s^{-1}) would correspond to H-atom abstraction from the −OC(O)H group. Assuming that the H atom and CH_3 group have only a small influence on the reactivity of the *tert*-butyl group in the *tert*-butyl formate and *tert*-butyl acetate, respectively, the contribution of H-atom abstraction from the −OC(O)H group to the overall rate constant can be calculated as follows:

$$k(\mathrm{H}) = k(\mathrm{OH} + \mathrm{HC(O)OC(CH_3)_3}) - [k(\mathrm{OH} + \mathrm{CH_3C(O)OC(CH_3)_3}) - k(\mathrm{CH_3})] = 2.86 \times 10^{-13}$$

where $k(CH_3)$ is the contribution of the $CH_3C(O)$ group to the overall rate constant k(OH + $CH_3C(O)OC(CH_3)_3$) and is taken as $k(CH_3) = 1.0 \times 10^{-13}$ (half of the experimental rate constant value for the reaction OH + acetone: k(OH + $CH_3C(O)CH_3$) = 2.19×10^{-13}, recommended value,[17] and $(1.84 \pm 0.24) \times 10^{-13}$, recently obtained in our laboratory[18]). The higher value of the partial rate constant of the −OC(O)H group in *tert*-butyl formate, $(2.43-2.86) \times 10^{-13}$, compared to that in methyl formate, 0.9×10^{-13}, may be explained by a higher positive inductive effect of the *tert*-butyl group in *tert*-butyl formate compared to the methyl group in methyl formate. From the above discussion, it may be speculated that the nature of the R_1 group in the ester $R_1C(O)OR_2$ influences the reactivity of the R_2 group and vice versa.

Temperature Dependence of the OH + Formate Reaction Rate Constants. The rate constants k_1 and k_5 exhibit a weak positive temperature dependence as previously observed in our laboratory for the rate constant of OH reactions with ethers and esters containing only methyl groups: dimethyl ether (CH_3OCH_3),[10] methyl *tert*-butyl ether ($CH_3OC(CH_3)_3$),[19] methyl acetate ($CH_3C(O)OCH_3$),[14] and *tert*-butyl acetate ($CH_3C(O)O(CH_3)_3$).[15] If it is assumed that the temperature dependence of k_1 and k_5 is mainly controlled by H-atom abstraction from CH_3 groups, the present data, then, further confirms that H-atom abstraction from a CH_3 group has a positive temperature dependence.

Although the Arrhenius plots for k_2, k_3, and k_4 are correctly fitted by a straight line with a near zero (k_3 and k_4) or very slightly negative slope (k_2), slight curvatures of the plots cannot be excluded as clearly observed in the same range of temperature for methyl acetate and ethyl acetate.[13,14] The curvature in the Arrhenius plots probably arises from differences in the temperature dependencies of the individual rate constants for OH attack at different sites in the formates. Also, a second pathway forming a long-lived adduct by OH addition to the carbonyl group cannot be excluded specially at low temperatures and low pressures. This was for instance suggested for OH reaction with aliphatic ketones.[20] However, the occurrence of such a mechanism could not be firmly established since no pressure dependencies of the rate constants were observed.

Atmospheric Implication

With a typical tropospheric OH concentration of 1×10^6 molecules cm^{-3} the following tropospheric lifetimes ($\tau = 1/k_i$[OH]) are calculated (in days): 66.9, 13.6, 6.4, 3.3, and 15.5 for methyl formate, ethyl formate, *n*-propyl formate, *n*-butyl formate, and *tert*-butyl formate, respectively. These lifetimes are fairly long and mean that the formates may be transported far from their emission locations. In particular, urban and suburban emissions of these compounds are unlikely to contribute to local ozone and photooxidant formation. The lifetimes of the studied formates are also significantly higher than those of the ethers which produce them as intermediates in their atmospheric oxidation mechanisms. The lifetimes for the precursor ethers are 4 days for dimethyl ether (methyl formate), 1 day for diethyl ether (ethyl formate), 3.7 days for methyl *tert*-butyl ether (*tert*-butyl formate), and 1.3 days for ethyl *tert*-butyl ether (*tert*-butyl formate).[10,19] Thus, the capacity of these ethers to form ozone and other oxidants is not only limited by their OH-initiated oxidation but also in part by the OH-initiated oxidation of the formates generated in the primary process.

Acknowledgment. French Ministry of Environment and European Commission for support.

References and Notes

(1) Japar, S. M.; Wallington, T. J.; Richert, J. F. O.; Ball, J. C. *Int. J. Chem. Kinet.* **1990**, *22*, 1257−1269.

(2) Japar, S. M.; Wallington, T. J.; Rudy, S.; Chang, T. Y. *Environ. Sci. Technol.* **1991**, *25*, 415−420.

(3) Tuazon, E. C.; Carter, W. P. L.; Aschmann, S. M.; Atkinson, R. *Int. J. Chem. Kinet.* **1991**, *23*, 1003−1015.

(4) Smith, D. F.; Kleindienst, T. E.; Hudgens, E. E.; McIver, C. D.; Bufalini, J. J. *Int. J. Chem. Kinet.* **1991**, *23*, 907−924.

(5) Smith, D. F.; Kleindienst, T. E.; Hudgens, E. E.; McIver, C. D.; Bufalini, J. J. *Int. J. Chem. Kinet.* **1992**, *24*, 199−215.

(6) Langer, S.; Ljungström, E.; Wängberg, I. *J. Chem. Soc., Faraday Trans.* **1993**, *89*, 425−431.

(7) Atkinson R.; Carter, W. P. L. *Chem. Rev.* **1989**, *84*, 437.

(8) Calvert J.; Pitts Jr. J. N. *Photochemistry*; Wiley: New York, 1966.

(9) Mellouki, A.; Téton, S.; Laverdet, G.; Quilgars, A.; Le Bras, G. *J. Chim. Phys.* **1994**, *91*, 473−487.

(10) Mellouki, A.; Téton, S.; Le Bras, G. *Int. J. Chem. Kinet.* **1995**, *27*, 791−805.

(11) Vésine, E.; Mellouki A. *J. Chim. Phys.* **1997**, in press.

(12) Wendt, H. R.; Hunziker J. *Chem. Phys.* **1979**, *71*, 5202−5205.

(13) Wallington, T. J.; Dagaut, P.; Liu, R.; Kurylo, M. J. *Int. J. Chem. Kinet.* **1988**, *20*, 177−186.

(14) El Boudali, A.; Le Calvé, S.; Le Bras, G.; Mellouki, A. *J. Phys. Chem.* **1996**, *100*, 12364−12368.

(15) Le Calvé, S.; G. Le Bras, G.; Mellouki, A. *Int. J. Chem. Kinet.*, **1997**, in press.

(16) Kwok, E. S. C; Atkinson, R. *Atmos. Environ.* **1995**, 29, 1685−1695.

(17) Atkinson, R. *J. Phys. Chem. Ref. Data* **1994**, Monograph 2.

(18) Le Calvé, S.; Hitier, D.; Le Bras, G.; Mellouki, A., to be submitted for publication.

(19) Téton, S.; Mellouki, A.; Le Bras, G.; Sidebottom, H. *Int. J. Chem. Kinet.* **1995**, *28*, 291−297.

(20) Wallington, T. J.; Kurylo, M. J. *J. Phys. Chem.* **1987**, *91*, 5050−5054.